High-Speed Far-Field Energy Measurements in a 9-kW Hall Effect Thruster for Model Inference and Calibration

Austen Thomas[1] and Kristina Lemmer[2]
Western Michigan University, Kalamazoo, MI, 49009, United States
Janice Cabrera[3] and Mitchell L. R. Walker[4]
Georgia Institute of Technology, Atlanta, GA, 30332, United States
Tyler Topham[5] and John Foster[6]
University of Michigan, Ann Arbor, MI, 48109, United States

This investigation presents far-field ion energy measurements utilizing a high-speed retarding potential analyzer in the plume of the H9, a 9-kW Hall effect thruster (HET). The purpose of the presented work is to demonstrate the ability of a high-speed diagnostic to measure oscillations in ion energy in a high-powered HET around the frequency of the breathing mode. The H9 was operated on krypton at the 600 V, 15 A thruster operating condition. The facility's pressure remained below 6 x 10^{-6} Torr-Kr. A standard retarding potential analyzer was used in conjunction with high-speed circuitry to capture time-resolved resolved ion energy distribution functions (IEDFs) at two positions within the plume of the H9. The oscillations observed in the time-resolved IEDFs display a periodic behavior aligning with breathing mode characteristics oscillating at a frequency of at 19.2 kHz. These oscillations were shown to decrease in mean ion energy but increase in peak-to-peak oscillations as the radial position of the probe was increased. We demonstrate the capability of the HRSPA to measure high-speed ion energy oscillations within the plume of the H9, where we observe several temporally oscillating ion energy populations. As expected, a mean most probable energy of 578 eV with 55 eV peak-to-peak oscillations was measured in the time-resolved IEDFs at the centerline location, aligning with the 600V, 15 A operating condition. The time-resolved IEDF at the off-centerline line location measured lower a mean most probable ion energy of 454 eV with greater peak-to-peak oscillations of 156 eV. Data obtained from this experiment are meant to inform upon predictive engineering models (PEMs) being developed by the Joint AdvaNced PropUlsion InStitute (JANUS), enhancing our understanding of HET behavior.

Nomenclature

A	Aperture area
D	Embedding dimension
E	Ion energy
e	Elementary charge
f	Distribution function
I_{coll}	Collector current
k	Nearest neighbors
m_i	Ion mass
N	Sample depth
n_i	Ion density
T_e	Electron temperature
V_{bias}	Retarding potential
V_p	Plasma potential
τ	Time-lag

[1] Ph.D. Candidate, Mechanical Engineering, and AIAA Student Member.
[2] Professor, Mechanical & Aerospace Engineering, and AIAA Associate Fellow.
[3] Graduate Student, School of Aerospace Engineering, and AIAA Student Member.
[4] Professor, School of Aerospace Engineering, and AIAA Fellow.
[5] Ph.D. Candidate, Nuclear Engineering & Radiological Sciences, and AIAA Student Member.
[6] Professor, Nuclear Engineering & Radiological Sciences, and AIAA Associate Fellow.

I. Introduction

Hall effect thrusters (HETs) have been the focus of electric propulsion (EP) research since their inception. At present, there is a significant ongoing effort to investigate high-power HETs and the impact of testing in ground-based facilities. The Joint AdvaNced Propulsion InStitute (JANUS), a NASA Space Technology Research Institute was created to address the impact of ground testing on high-power EP thrusters, through the combination of experimental investigations in ground-based testing facilities and predictive engineering models (PEMs). A primary objective of JANUS is to account for facility effects within the PEMs. As EP thrusters rise in power, limitations of ground-based testing facilities may be reached, where the environment produced within these facilities is no longer indicative of space operation, resulting in data that lack practical value. As such, PEMs must be used in place of expensive and time-consuming ground testing and to predict in-space behavior based on limited ground testing. Presently, one of the key hurdles facing the accurate assessment of thruster performance using PEMs is the presence of extreme facility effects encountered when testing high-power, high-flow rate EP thrusters in ground-based vacuum facilities [1]. The work presented here furthers the efforts of JANUS by measuring populations of temporally oscillating ions at varying energy levels in the far field plume of a 9-kW level HET to provide data to inform the models.

Characterization of the evolving state of a plasma is required if a thorough understanding of HET dynamics is desired. Measurements of temporal ion energy provide a means to precisely quantify the influence of ion energy oscillations on the erosion and performance of EP thrusters. Techniques such as time-resolved laser-induced fluorescence (TRLIF) measurements have proven effective at obtaining time-resolved ion velocity distribution functions (IVDFs) [2–5]. While TRLIF is an effective tool, it is expensive, time-consuming, and cannot be implemented onboard spacecraft Recent developments utilizing a standard retarding potential analyzer (RPA) in conjunction with high-speed circuity have demonstrated the capability of producing time-resolved IEDFs allowing the influence of temporal ion energy to be studied [6, 7]. RPAs are an electrostatic diagnostic tool that utilize a series of electrically-biased mesh grids to establish a potential barrier to impinging ions, screening ions with energy less than the sourced potential. Their simplicity in design and operation makes RPAs an accessible and valuable tool for experimental plasma measurements.

A high-speed retarding potential analyzer (HSRPA) is an RPA that utilizes high-speed circuity combined with data fusion techniques to obtain time-resolved measurements. An HSRPA operates similarly to a traditional time-averaged RPA, excluding how collector current measurements are performed and data post-processing. High-speed measurements of collector current are recorded while holding the retarding grid at a constant bias. Simultaneously, a second measurement, which is coupled to the plasma source is measured. After a specified amount of data have been recorded, the retarding grid potential is then increased by an appropriate voltage step size to obtain the desired IEDF resolution. The collector current and secondary measurement coupled to the source are then sampled again, recording the same amount of data. This process is repeated until a complete potential distribution is achieved. Postprocessing requires the establishment of a map between a system input and output, which is then used to create reconstructed waveforms producing a time-resolved IEDF. In this work, the RPA collector current was used as the output, and the HET discharge voltage was used as the input. The discharge voltage signal is mapped to each corresponding collector current signal at each retarding grid potential. The combination of these maps results in a set of reconstructed waveforms that have been pseudo-triggered simultaneously, forming a time-resolved IEDF [6]. The data obtained from HSRPA measurements in this investigation will enable the inference and calibration of PEMs being developed by JANUS.

The following sections present details on the work completed with a four-grid RPA to generate time-resolved ion energy measurements within the plume of the H9 HET operating at 9.0 kW (600 V, 15 A) on krypton propellant. The organization of this paper is as follows. First, the experimental setup is discussed in Section II, including the facility, test article, and diagnostics used to complete this work. Sections III and IV present the results obtained and a discussion of those results, respectively. Lastly, Section V provides the final comments and conclusion of this investigation.

II. Experimental Setup

The experiment was conducted at the Georgia Institute of Technology as part of a JANUS test campaign. Several universities participated in the campaign, each of which completed a separate investigation. This collaboration furthers

the efforts of JANUS to quantify the impact of facility effects on EP thruster operation. Below the facilities, thruster, and diagnostics used in this investigation to complete time-resolved ion energy measurements are discussed.

A. Facility

All testing was completed at the Georgia Institute of Technology at the High-Power Electric Propulsion Laboratory (HPEPL). Vacuum Test Facility 2 (VTF-2), a 4.9-m-diameter by 9.2-m-long cylindrical vacuum chamber, was utilized during this test campaign. VTF-2 is capable of achieving a base pressure of 1.9×10^{-9} Torr by employing a cryogenic pumping system. Background pressure was monitored by two ion gauges: a Varian 571 ion gauge and a 3701120 Stabil-ion gauge located behind the thruster. Propellant flow rates were regulated by two MKS GE50A flow controllers. During HSRPA measurements, operating pressure remained below 6×10^{-6} Torr-Kr.

B. Thruster

The testing campaign utilized the H9, a 9-kW magnetically shielded HET, developed through a collaboration between the Jet Propulsion Laboratory (JPL), the University of Michigan, and the Air Force Research Laboratory (AFRL) [8]. The H9 serves as a common test article for JANUS experiments aimed at investigating the impact of facility effects on high-power HETs. Figure 1 shows an image of the H9 operating during this campaign. The design and acceptance testing of the H9 is extensively covered in Ref. [8], addressing essential features including the geometry of the discharge chamber, anode/gas distributor, cathode, and magnetic circuit.

For the presented work, the H9 was operated at 9.0 kW (15 A, 600 V) with krypton propellant. The flow rate was 184 – 188 sccm to the anode and 12.88 - 13.12 sccm to the cathode. The thruster was mounted at the centerline of the vacuum facility and fired downstream at a graphite beam dump. To monitor the time-resolved discharge characteristics of the thruster including voltage and current, a Powertek DP25 high-voltage probe and an 804 Pearson coil were utilized, respectively.

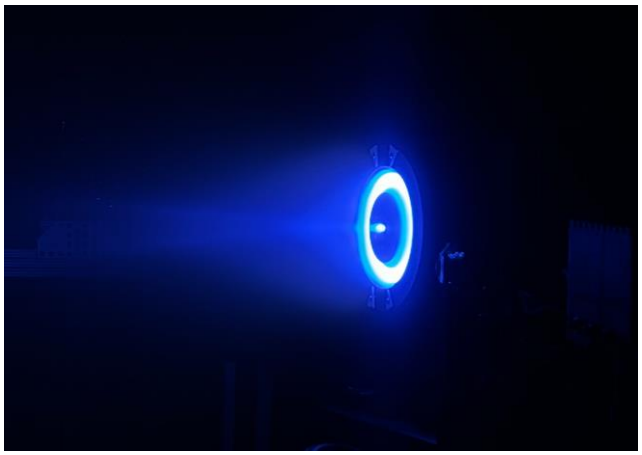

Fig. 1 H9 operating on Krypton at 9kW.

C. Probes

The diagnostics used in this investigation, including an HSRPA, emissive probe, and Langmuir probe, were placed on a linear motion stage 2-m-downstream of the thruster, raised on an 80/20 T-slotted mounting arm, and fixed at centerline height. Additionally, a transimpedance amplifier (TIA) was mounted to the back of the RPA within the vacuum chamber, allowing line capacitance to be minimized between the RPA and TIA. The linear motion stage enabled the probes to be moved to select radial positions within the plume of the H9. Figure 2 illustrates the experimental setup utilized in this investigation. The following sections describe the setup and functionality of each diagnostic tool.

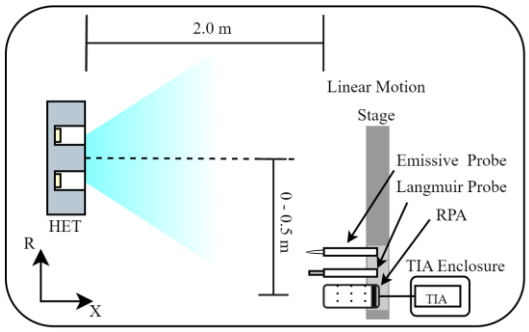

Fig. 2 Simplified experimental setup.

i. Retarding Potential Analyzer

An RPA functions by establishing a variable electric field normal to impinging ions, creating a potential barrier below which ions are filtered with energy less than the sourced potential. The electric field within the RPA is established by biased mesh grids. The RPA utilized in this investigation is a four-grid configuration, composed of three electrostatically biased mesh grids and a floating grid in front of the current collection plate. The body, grids, retention rings, and wires are composed of 316 stainless steel. MACOR washers and a MACOR inner sleeve were employed to insulate the grids from the RPA body and each other, while alumina tubing insulated the wires connected to the grids. Figure 3 shows the RPA schematic. Briefly, Grid 1 is floating to minimize disturbance to the plasma. Grid 2 is biased negatively to repel plasma-born electrons from entering the RPA. Grid 3 is the retarding grid responsible for filtering ions. Grid 4 is biased negatively to suppress electron emission from the grids and collector due to the impact of high-energy ions. The RPA utilized in this investigation possesses an energy resolution, as determined by the geometry of the RPA grids, of approximately 1% of the retarding grid potential [9]. Further details on the construction of the RPA can be found in Ref [10].

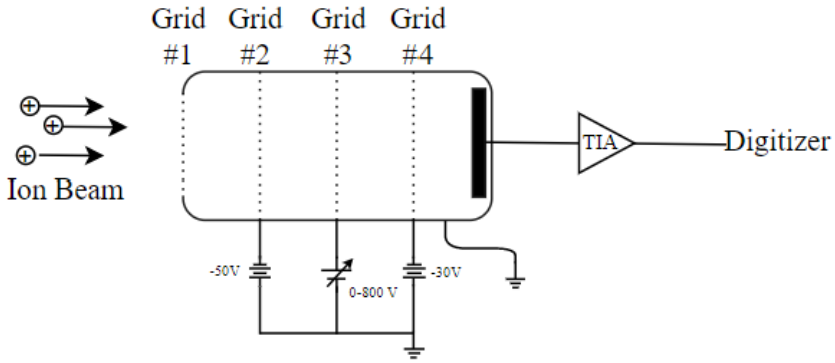

Fig. 3 Retarding potential analyzer setup [7].

Operationally, the retarding grid is swept over a range of potentials, filtering ions based on their energy. Ions with an energy exceeding the potential barrier can pass through the retarding grid and arrive at the collector, forming a measurable current. A relationship between the measured collector current and sourced retarding grid potential can be established, forming an I-V trace. The negative first derivative of the collector current with respect to the retarding grid bias is directly proportional to the IEDF given by,

$$\frac{dI_{coll}}{dV_{bias}} = -Aen_i\sqrt{\frac{2E}{m_i}}f(E). \tag{1}$$

Equation (1) is commonly approximated solely as the derivate of the collector current with respect to the retarding grid bias as it is the shape of the distribution function, rather than the magnitude, that is of concern.

$$f(E) \approx -\frac{dI_{coll}}{dV_{bias}} \tag{2}$$

The measurements collected in this investigation were performed at 133 discrete retarding grid potentials. The retarding bias profile was $V_{bias} = [0{:}\,10{:}\,530\ 531{:}\,1{:}\,600\ 610{:}\,10{:}\,700]$ V, and it was chosen to optimize the capture of discharge oscillations occurring near the thruster discharge voltage. The retarding grid was swept by a Keithley 237 source measurement unit, while the repelling and suppression grids were biased with a set of batteries to a potential of -50 V and -40 V, respectively. Collector current measurements were obtained using a FEMTO DHPCA-100 commercial TIA, featuring a bandwidth of up to 200 MHz. Time-resolved RPA measurements were performed as follows: High-speed collector current measurements were sampled at 500 MS/s while holding the retarding grid at a constant potential. Simultaneously, the discharge current was measured until a sample depth of 1.4 MS was recorded. This was repeated for each retarding bias in the profile.

Time-series data reconstruction is achieved using data fusion techniques such as shadow manifold interpolation (SMI) or the Empirical transfer function method [11, 12]. This investigation utilized SMI to achieve time-series data reconstruction, which employs a non-linear approach based on manifold reconstruction techniques and convergent cross-mapping (CMM) from Takens and Sugihara, respectively [13, 14]. This method requires shorter data sets than the transfer function method while still effectively reconstructing non-sinusoidal features [11]. In this investigation, the SMI parameters were chosen to achieve the highest correlation value and, therefore, varied slightly between reconstructions. The training and testing sample depth, the embedding dimension, and the nearest neighbors were all held constant at N = 30 kS, D = 12, and k = 100. The time-lag varied between data sets and was set to τ = 6 - 7 samples Details on SMI and its parameters can be found in Refs [6, 7, 11]. The reconstructed waveforms are assembled to form I-V curves at each representative point in time. Subsequently, signal noise was reduced by applying a smoothing spline to the reconstructed I-V curves, and time-resolved IEDFs were determined using Equation (2).

ii. Langmuir Probe

A single Langmuir probe was utilized to obtain time-averaged plasma potential measurements for corrections to RPA ion energy. The probe consisted of a 1.5-mm-diameter pure tungsten wire placed within a double-bore alumina tube with 10 mm of length exposed. These dimensions were chosen to maintain a thin sheath assumption [15]. To determine the time-averaged plasma potential, the Langmuir probe was swept from -30 V to 30 V while the current to the probe from the plasma was measured, forming an I-V curve. The plasma potential is located at the inflection point, or knee, of the I-V curve and is determined by differentiating the I-V curve and identifying the maximum value of the derivative. The true ion energy from the RPA is calculated using Equation (3).

$$E = eV_{bias} - eV_p \tag{3}$$

This correction is necessary as the retarding grid of the RPA is ground referenced. To ensure an accurate correction, the plasma potential was measured near the RPA, referred to as the local plasma potential. The Langmuir probe was positioned 100 mm from the RPA orifice, with this distance deemed sufficient as any spatial plasma potential variation over this distance is assumed to be insignificant, given the plasma potential gradient 2-m downstream of the thruster [16, 17]. Langmuir probe data analysis was conducted according to recommended practices by Lobbia *et al.* [15].

iii. Emissive Probe

A floating emissive probe was utilized in this investigation to obtain additional time-averaged and time-resolved plasma potential measurements. The probe was constructed following recommended practices by Sheehan, *et al.* and is depicted in Fig. 4 [18], [19]. Bored alumina tubing was used as the housing and isolating material. Bare strand 18 AWG copper wire was inserted along the full length of the bored holes of the alumina tube. A 0.0254-mm-diameter thoriated-tungsten wire was wedged into the copper strands in a hairpin configuration, extending 2-3 mm outwards. Ceramabond was applied over the copper wire to insulate it from the plasma. The emissive probe was located approximately 200 mm from the orifice of the RPA.

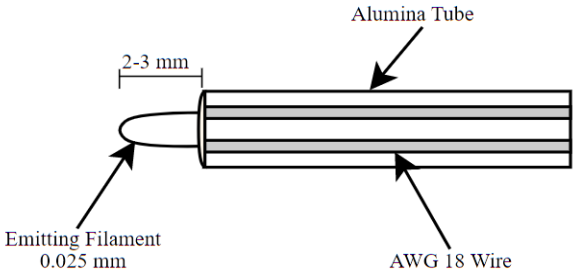

Fig. 4 Emissive probe design.

In this investigation, the floating emissive probe with the large emission method was selected for its simplicity and ability to provide temporal data. Other methods for obtaining the local plasma potential are described more rigorously by Sheehan *et al.* [18], [19]. Here it is sufficient to mention that the floating method offers reasonable accuracy of the plasma potential within $1.5T_e$ to $2.0T_e$ in plasmas with a density in the range of $10^{11} - 10^{18}\ m^{-3}$. In this work, direct joule heating was applied to induce electron emission from a 0.0254-mm-diameter thoriated-tungsten wire. This was achieved using four 6-volt batteries in parallel and a rheostat to control the voltage drop across the filament, controlling the emitted electron current. The circuit is disconnected from any ground references, allowing the filament to "float" to the local plasma potential when the emitted electron current from the wire equals the local plasma electron saturation current.

The plasma potential is determined by identifying the location where the floating potential saturates in the I-V curve. When the emitted current is significantly lower than the electron saturation current, the filament's potential remains close to the ground reference and changes slowly. As the emitted current approaches the electron saturation current, the filament potential increases rapidly until it reaches the plasma potential. Further increases in emitted current only result in a slight increase in the filament potential due to space charge effects, where an excess of emitted electrons forms a virtual cathode around the wire. Figure 5b depicts such an I-V curve measured in this work with the plasma potential occurring at the red marker. The plasma potential can be identified on the I-V trace, by either locating the inflection point of its derivative or using the method proposed by Kemp and Sellen, where the intersection of linearly fitted lines in the rapidly growing range and the saturation region is a reasonable fit [20]. From this point, extrapolating back to zero-current via the load line reveals the plasma potential, where the load line is the IV-trace if there is no plasma and would appear as a flat line in a simple resistor circuit as was done in this work.

To capture the temporal plasma potential, the filament is heated in excess of the electron saturation current, past the time-averaged plasma potential, and the fluctuations of the potential are monitored. The peak-to-peak plasma potential oscillations are then added to the time-averaged plasma potential measurement measured with the I-V curve, correcting for excess heating. It is important to enter sufficiently deep into the saturation region to accurately capture the entirety of the oscillation waveform, without going below the DC plasma potential. An insufficient emission current at a high plasma density may result in the probe being temporarily located in the rapidly increasing regime of the I-V trace, resulting in a drastically lower measured plasma potential. In this work, the high-speed plasma potential measurements were recorded with an 8-bit digital oscilloscope sampled at 500 MS/s to capture the desired plasma dynamics.

III. Results

A. Time-Averaged Measurements

Time-averaged measurements of ion energy and plasma potential were obtained from RPA, Langmuir probe, and emissive probe measurements. Measured I-V traces used to obtain plasma potential are shown in Fig. 5a (Langmuir probe) and Fig. 5b (emissive probe). The plasma potential measurements obtained with the Langmuir and emissive probes can be seen in Fig. 5, denoted by the red markers. Relatively good agreement is observed with time-averaged plasma potential measurements at both positions. A summary of time-averaged data measured at each location is shown in Table 1. As expected, the plasma potential decreases further from the thruster centerline [21]. The measured ion energy from the RPA will be corrected by these plasma potential measurements as indicated in Equation (3).

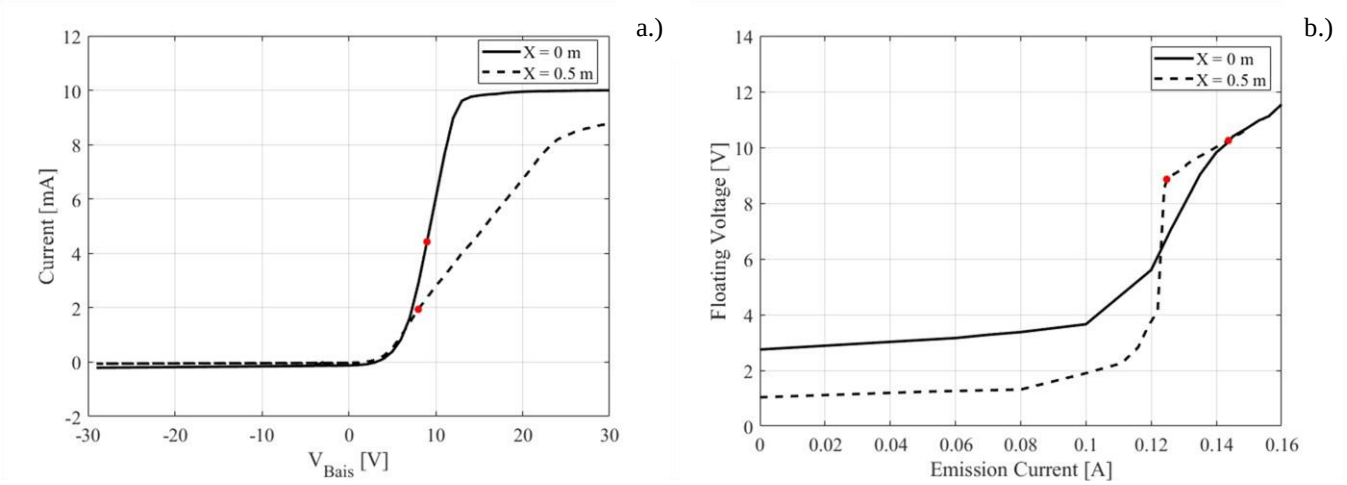

Fig. 5 Time-averaged (a) Langmuir probe and (b) emissive probe data at centerline and 0.5 m from centerline for 600 V, 15 A condition.

Table 1 Time-averaged data points for H9 at for 600 V, 15 A.

	Centerline	**0.5-m-off Centerline**
Discharge Voltage	600 V	600 V
Discharge Current	15 A	15 A
Langmuir Probe Plasma Potential	9 V	8 V
Emissive Probe Plasma Potential	10.2 V	8.8 V
FWHM	99 eV	232 eV
Most Probable ion energy (corrected)	582 eV	461 eV

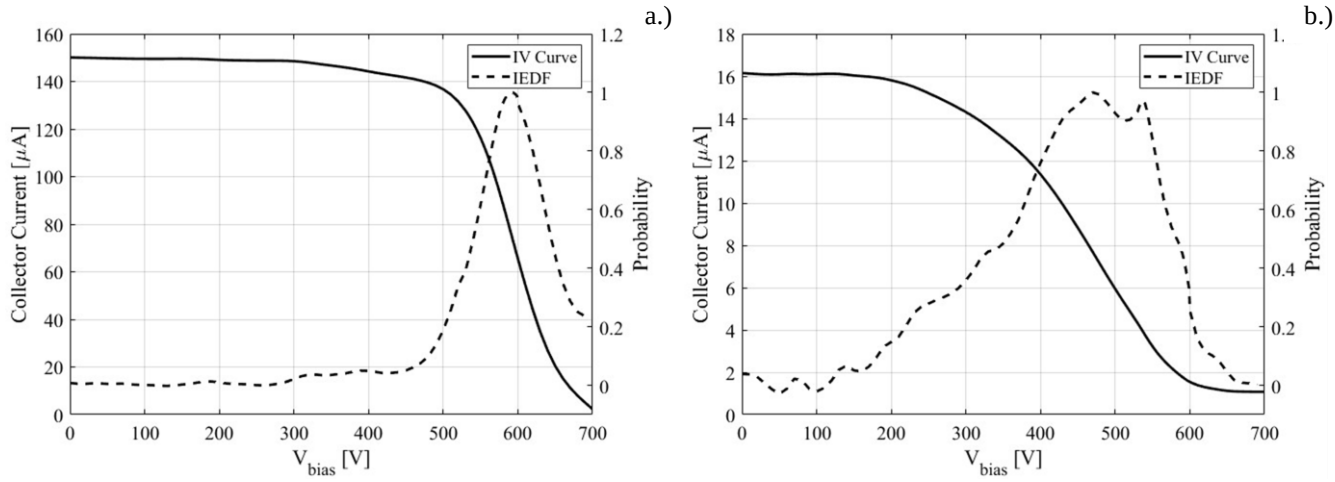

Fig. 6 Time-averaged RPA I-V curves and IEDFs at (a) centerline and (b) 0.5 m from centerline for 600 V, 15 A condition.

B. Time-Resolved Measurements

High-speed emissive probe floating voltage measurements were conducted to estimate plasma potential fluctuations, aiming to correct peak-to-peak ion energy measurements. These results are shown in Fig. 7. An approximation for peak-to-peak plasma potential oscillations was obtained from a period of roughly four breathing mode cycles, by calculating the maximum peak-to-peak amplitude of the plasma potential over this period. The floating voltage of the probe, or plasma potential, oscillates at the breathing mode frequency of approximately 19.2 kHz, aligning with expectations. The maximum peak-to-peak amplitude of the plasma potential estimated over this period at the centerline and 0.5 m from the centerline are 2.4 V and 1.7 V, respectively.

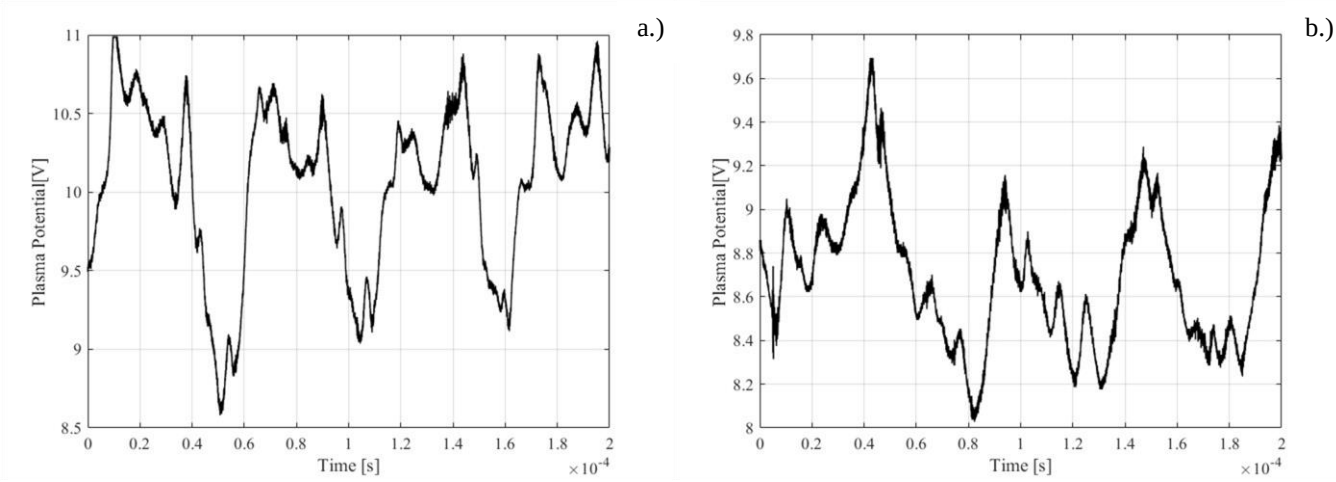

Fig. 7 Time-resolved emissive probe plasma potential measurements at centerline (a) and 0.5 m from centerline (b) for 600 V, 15 A condition.

Figure 8 shows the time-resolved IEDFs at a position 2-m-downstream along the centerline, while Fig. 9 shows the IEDFs at a position 2-m-downstream and 0.5-m from the centerline. The standard deviation between all time-resolved I-V curves remained low, with a maximum value of 59 nA at the centerline and 76 nA off the centerline. These low values were a result of a consistent current collection for a given retarding bias. First, in Fig. 8 the IEDF displays a pronounced sinusoidal behavior, oscillating at the breathing mode frequency, approximately 19.2 kHz. A mean ion energy of 578 eV is calculated with 55 eV peak-to-peak oscillations. An additional ion energy population appears between 400-500 eV. The last notable feature is the presence of a low-energy population spanning 0-50 eV, which appears with a relatively low probability. In Fig. 9, the time-resolved IEDF off the centerline exhibits a similar oscillatory nature, also occurring at the breathing mode frequency, albeit with considerably larger peak-to-peak oscillations. The mean ion energy was found to be around 454 eV with peak-to-peak amplitudes of 156 eV. Another

ion energy population is measured between 250 and 300 eV, appearing just below the troughs of the primary population of ions, that also correlates with the breathing mode frequency. Additionally, the lower ion energy population between 0-50 eV, which appears with only a low probability in the centerline position, is notably more prevalent off-centerline. Figures 10 and 11 offer an expanded view of the IEDFs alongside a plot of the discharge current measurement and are meant to provide insight into how oscillations in discharge current may correlate with the measured collected current and consequently time-resolved IEDFs. It is observed that the oscillations in ion energy within the IEDFs are lagging the discharge current measurement by approximately 55 μs, attributed to a time delay discussed further in Section IV.

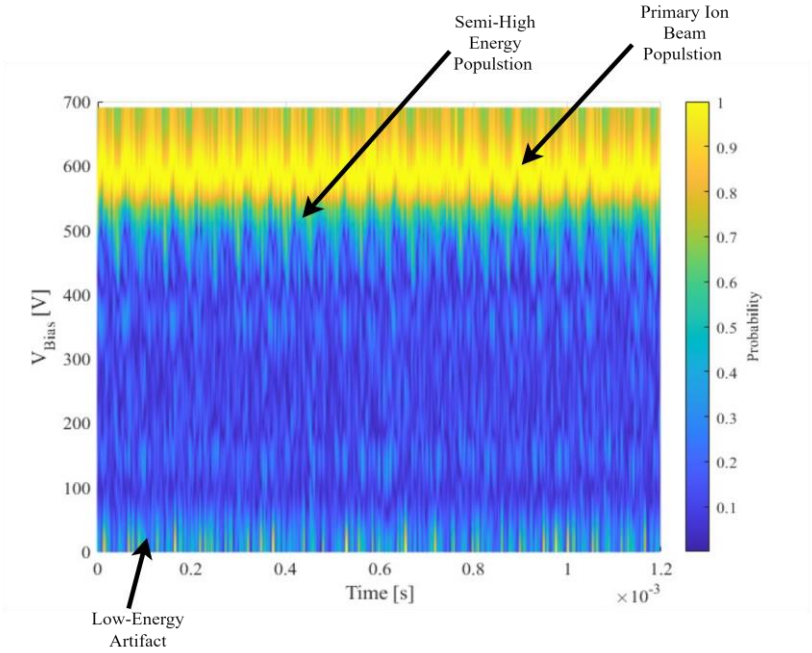

Fig. 8 Time-resolved IEDFs at centerline for 600 V, 15 A condition.

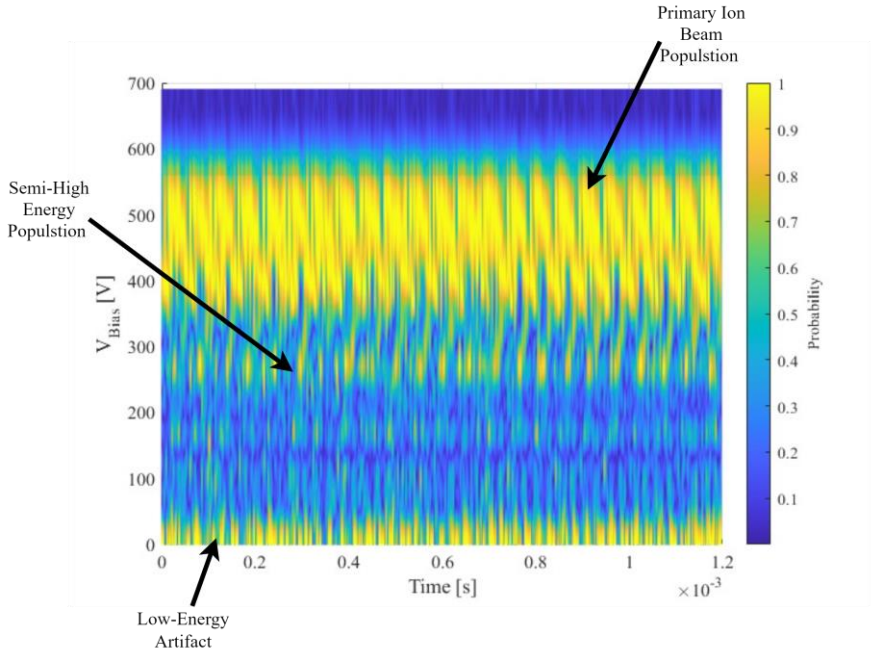

Fig. 9 Time-resolved IEDFs 0.5 m from centerline for 600 V, 15 A condition.

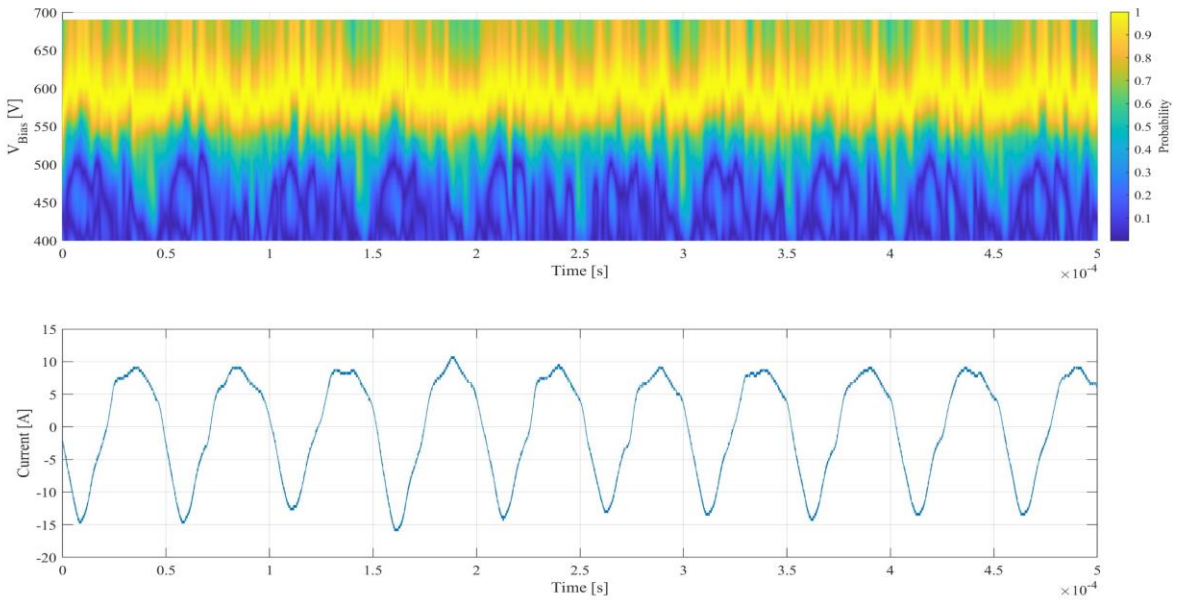

Fig. 10 Time-resolved IEDFs and AC discharge current at centerline for 600 V, 15 A condition.

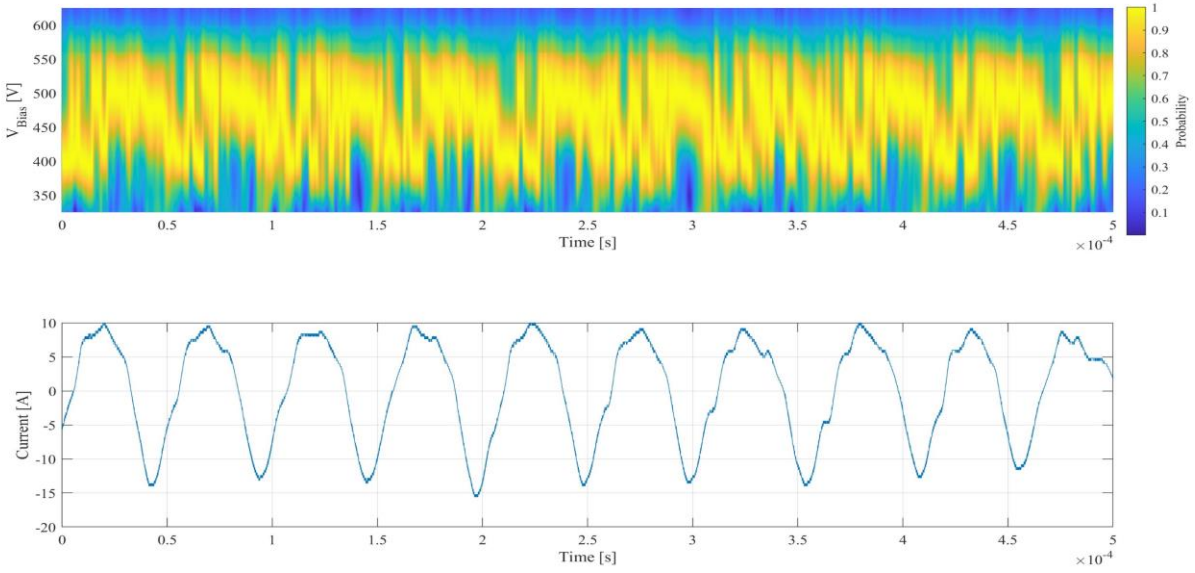

Fig. 11 Time-resolved IEDFs and AC discharge current 0.5 m from centerline for 600 V, 15 A condition.

IV. Discussion

The preceding section presented time-averaged and time-resolved measurements of plasma potential and most probable ion energy within the plume of the H9 HET operating on krypton at 9.0 kW, 2-m downstream at two radial positions: along the centerline and 0.5 m away from the centerline. The data obtained from this investigation will

enable the inference and calibration of PEMs being developed by JANUS. Furthermore, these findings demonstrate the ability of an HSRPA to measure ion energy fluctuations within the plume of high-power HETs at frequencies that correspond to the thruster breathing mode frequency.

A. Langmuir & Emissive Probe

Time-averaged data were collected to provide a foundation for comparison with the averaged measurements obtained from time-resolved data. Several elements are important to note when examining the time-resolved Langmuir probe and emissive probe data. There exists a small discrepancy of ~1 V between the Langmuir probe and emissive probe time-averaged plasma potential measurements. Notably, the plasma potential obtained from the emissive probe is regarded as more precise, due to its suitability for EP applications and its ability to acquire measurements with greater precision, particularly in a flowing plasma [15]. When using either Langmuir or emissive probes, the plasma potential is determined by identifying the location where saturation of the I-V curve occurs. The uncertainty of identifying the location or measuring the plasma potential with both probes is dependent upon several factors unique to the experimental environment, including probe construction and inherent noise of the plasma [22]. An investigation comparing the accuracy of Langmuir and emissive probe plasma potential measurements in a HET showed that the Langmuir probe possessed the greatest uncertainty of $0.5T_e/e$. The floating emissive probe method possessed an uncertainty of $0.1T_e/e$ of the floating potential and an additional error of $\sim T_e/e$ for plasma potential, which was still less than the uncertainty of the Langmuir probe measurement [22].

Comparing the time-averaged emissive probe measurements with the mean of the time-resolved measurements reveals a larger discrepancy of 1.5 V at the centerline and 1.2 V at 0.5 m from the centerline. This discrepancy arises from the need to heat the filament in excess of the electron saturation current to capture the plasma potential oscillations. Consequently, an increase in the emission current results in a corresponding rise in the floating voltage of the probe measurement. A sufficiently large increase in emissive current is required to accurately capture the plasma potential oscillations. Although it is common in the floating potential method to emit excessively and assume this is the plasma potential, there is a slight offset that occurs when compared with the plasma potential found from the knee of a full I-V trace. To account for the offset caused by the difference between time-averaged and the mean of time-resolved measurements, a correction is required for the mean of the time-resolved emissive probe measurement. This correction potential is the difference between the time-averaged and mean of the time-resolved measurement. Analyzing the time-resolved plasma potential measurements, the peak-to-peak amplitude of the plasma potential constantly changes overtime at the breathing mode frequency. Therefore, only an estimate of the peak-to-peak plasma potential is provided and is found by calculating the maximum peak-to-peak difference within the signal measured by the emissive probe. As the peak-to-peak oscillations were only on the order of ±1 V these corrections have little impact on altering the amplitude of the ion energy oscillations as the scale of the measured ion energy is oscillations was on the order of 10 eV or greater. Additionally, the oscillations in the plasma potential are on the order of the energy resolution of the RPA. As such, no corrections were applied to the peak-to-peak amplitude of the ion energy.

B. Retarding Potential Analyzer

Figure 6 displays time-averaged IEDFs obtained by averaging all current samples measured at a single retarding bias and stitching the averaged values together forming the I-V curve. These IEDFs exhibit significant differences between the centerline and 0.5-m off the centerline locations. The IEDF at 0.5-m off centerline is a much broader IEDF in terms of FWHM, compared to that measured at the centerline position. The FWHM at 0.5-m from the centerline is 133 eV greater than the FWHM calculated at the centerline. This indicates an additional ion energy population below the measured most probable ion energy is likely present in the wings of the plasma plume. The increase in width of the IEDF can also be observed by the more gradual decline in measured ion current observed in Fig. 6b with an average decline of -0.013 μA/V as opposed to the sharp decline observed in Fig. 6a of -0.118 μA/V. Such broadening is expected as the plasma plume contains more ions created at lower electric potentials and momentum is lost in more elastic collisions [23, 24]. Additionally, the drop in most probable ion energy observed between Fig. 6a and Fig. 6b is a result of only the normal energy component of the ions being slowed, while the parallel energy component is unaffected [9].

When comparing the time-averaged and time-resolved IEDFs, several interesting features are observed. As stated, at the centerline, the time-averaged IEDF possesses a 57% narrower distribution (Fig. 6a) than the IEDF measured at the off-centerline location. Inspecting the corresponding time-resolved IEDF of Fig. 8, the peak-to-peak ion energy oscillations are smaller in magnitude compared to the oscillations in the IEDF of the off-centerline location. In the

off-centerline location, the time-averaged IEDF has a broad distribution (Fig. 6b), and the time-resolved IEDF for the same off-centerline case has a similarly broad distribution, reflected by the higher magnitude of the peak-to-peak oscillations in the ion energy (Fig. 9). This comparison is intended to show that the FWHM of the time-averaged IEDF is correlated with the magnitude of the peak-to-peak ion energy oscillations of the time-resolved IEDF.

When examining the time-resolved IEDFs, several ion energy populations become apparent. The first is the primary beam ions oscillating at the breathing mode frequency of 19.2 kHz. Notably, a secondary higher frequency signal at approximately 78.5 kHz can be observed in Fig. 8 superimposed over the primary beam oscillation. These peaks are more easily observed in the enlarged IEDFs of Fig. 10 and Fig. 11. As the ion energy is directly linked to the accelerating potential, and therefore, the discharge voltage, these peaks are possibly a result of oscillations within the discharge voltage. An example of a discharge voltage trace measured in this work is shown in Fig. 12. The dominant frequency component is at 19.2 kHz; however, a higher frequency signal at 78.2 kHz is also present that could explain additional peaks in the time-resolved IEDFs.

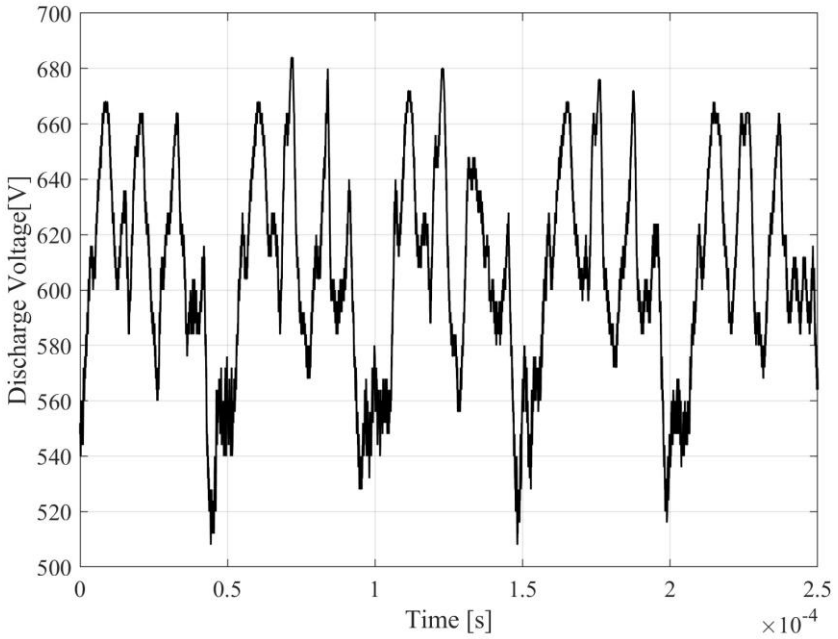

Fig. 12 Discharge voltage measurement for 600 V, 15 A condition.

A second population of low-energy ions is observed in the time-resolved IEDFs around 0 – 50 eV. These low-energy ions, not observed in the time-averaged IEDFs, appear in the time-resolved data. Figure 9 prominently shows this low-energy population in the off-centerline location, where this population is less obvious in the centerline location (Fig. 8). This could signify the onset of the CEX ion population; however, the CEX collision mean free path is several meters greater than the downstream location of the RPA within the plume. Therefore, it is more likely these populations are an artifact of the reconstruction process or RPA geometry. Additional ion energy populations exist in both the centerline and off-center IEDFs that oscillate with the breathing mode. At the centerline, this population exists between 400 – 500 eV, and at 0.5-m off the centerline, it exists between 200 – 300 eV. As stated with the time-averaged IEDFs, these lower ion energy populations could be the result of elastic collisions or ions originating from a region of lower acceleration potential.

The absence of prior high-speed ion energy measurements conducted with an RPA within the plume high-power HETs prevents a comparative analysis of past data. As mentioned in Section I, TRLIF has been used in previous investigations to study IVDFs in the plume of high-power HETs, showing that ion velocity oscillations correlate with temporal variations in the discharge current [3], [4]. When comparing the results obtained in this investigation with TRLIF measurements, we find similarities in the fluctuation of ion energy and velocity, each of which appears to

coincide with low-frequency oscillations of the breathing mode. However, TRLIF measurements were made either within or just outside of the thruster channel. The measurements presented in this work were made 2-m-downstream of the channel exit. Compared to LIF, RPAs offer a simple an effective way to measure temporal ion energy populations in the plume of HETs, and if mounted on a radial arm and swept azimuthally, could be utilized to investigate the entire HET plume.

The analysis of the time-resolved IEDFs reveals artifacts present stemming from post-processing steps such as SMI reconstruction and signal smoothing. These artifacts manifest as regions of moderate to low intensity in the time-resolved IEDFs and are highlighted in Fig. 13. While it is plausible these are true features of the IEDF, the authors believe these are a result of post-processing and suggest using a higher resolution for the retarding potential mitigate the issue. Additionally, a time delay exists between the oscillations observed in the reconstructed IEDFs and the measured discharge current oscillations. This delay arises from the time required for an ion to travel from the thruster channel exit to the RPA and the residence time within the RPA, before arriving at the collector. The transit time for a 578 eV ion to leave the thruster channel and travel approximately 2 m downstream is 54.6 μs. An additional delay on the order of 0.1 μs is caused by the time it takes an ion to transverse the non-zero electric field within the RPA. The combination of these delays results in a total time lag of is approximately 55 μs.

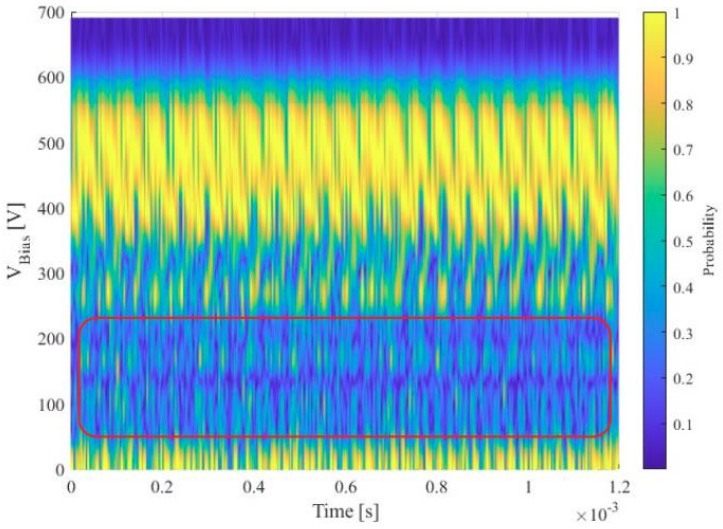

Fig. 13 Example of artifacts present in time-resolved IEDFs for 600 V, 15 A condition.

V. Conclusions

An HSRPA was used to successfully measure the evolution of ion energy in the far-field plume of a 9-kW magnetically shielded HET. Utilizing SMI, high-speed current measurements were reconstructed to provide time-resolved IEDFs. Data were measured at a distance 2-m-downstream of the thruster at two radial positions, along the centerline and 0.5-m off the centerline, while operating at 600 V and 15 A. The resulting time-resolved IEDFs showed temporal variations in ion energy which align with the breathing mode frequency. Average ion energy decreased as the RPA was moved further radially from the thruster centerline, while the magnitude of the peak-to-peak ion energy oscillations increased. While this work has produced satisfactory results, improvements to the measurements can be made in selecting a finer retarding grid bias resolution, more spatial locations, and more operating conditions. The data obtained from this investigation will be used to inform upon and calibrate thruster plume models that will be integrated into PEMs being developed by JANUS. Further experimentation with a 9-kW HET at the same operating conditions in a different facility should be carried out to better understand facility impact. This investigation has shown that an HSRPA can successfully be used to measure temporal ion energy oscillations within high-power HETs.

Acknowledgments

This work was partially supported by NASA through the Joint Advanced Propulsion Institute, a NASA Space Technology Research Institute, grant number 80NSSC21K1118.

References

[1] Wirz, R., Gorodetsky, A., Jorns, B., & Walker, M. Predictive Engineering Model for Life and Performance Assessment of High-Power Electric Propulsion Systems. Presented at the 37th International Electric Propulsion Conference. *Massachusetts Institute of Technology, Cambridge, MA USA. 2022.*

[2] Durot, C. "Development of a Time-Resolved Laser-Induced Fluorescence Technique for Nonperiodic Oscillations." Ph.D thesis, University of Michigan, (2016).

[3] Chaplin, V., Lobbia, R., Lopez, A., Mikellides I., Hofer R., Polk J., & Friss, A. (2020) Time-resolved ion velocity measurements in a high-power Hall thruster using laser-induced fluorescence with transfer function averaging. *Applied Physics Letters*, 116(23)https://doi.org/10.1063/5.0007161

[4] Roberts, P., Chaplin, V., Lopez, A., & Mikellides, I. (2022). Impact of low-frequency oscillations on ion energy in a high-power magnetically shielded Hall thruster. *Journal of Applied Physics*, *131*(3). https://doi.org/10.1063/5.0067325

[5] Durot, C., Gallimore, A., & Smith, T. (2014) Validation and evaluation of a novel time-resolved laser-induced fluorescence technique. *Review of Scientific Instruments*, 85(1)https://doi.org/10.1063/1.4856635

[6] Baird M., McGee-Sinclair R., Lemmer, K., & Huang, W. (2021) Time-resolved ion energy measurements using a retarding potential analyzer. *Review of Scientific Instruments*, 92(7)https://doi.org/10.1063/5.0039621

[7] Thomas, A. & Lemmer K Time-resolved Ion Energy Measurements Using A Retarding Potential Analyzer for Electric Propulsion Applications. *Review of Scientific Instruments*, *95*(2). https://doi.org/10.1063/5.0176167

[8] Hofer RR, Cusson SE, Lobbia RB, Gallimore AD The H9 Magnetically Shielded Hall Thruster. *Presented at the 35th International Electric Propulsion Conference. Georgia Institute of Technology, Atlanta, Georgia US 2017*

[9] Enloe, C. (1994) High-resolution retarding potential analyzer. *Review of Scientific Instruments*, 65(2):507–508. https://doi.org/10.1063/1.1145167

[10] Baird, M., Kerber, T., Lemmer, K., &Huang, W. Hall Thruster Plume Measurements of Time Resolved Ion Energy. Presented at the 36th International Electric Propulsion Conference. University of Vienna, Austria. 2019

[11] Eckhardt, D., Koo, J., Martin, R., Holmes, M., & Hara, K. (2019) Spatiotemporal data fusion and manifold reconstruction in Hall thrusters. *Plasma Sources Science and Technology*, 28(4)https://doi.org/10.1088/1361-6595/ab0b1f

[12] Lobbia, R. & Gallimore, A. (2008). A method of measuring transient plume properties. *44th AIAA/ASME/SAE/ASEE Joint Propulsion Conference and Exhibit*, https://doi.org/10.2514/6.2008-4650

[13] Takens, F. (1981) Detecting strange attractors in turbulence. :366–381. https://doi.org/10.1007/bfb0091924

[14] Sugihara, G., May, R., Ye, H., Hsieh, C., Deyle, E., Fogarty, M., & Munch, S. Detecting Causality in Complex Ecosystems. (2012). *Science (American Association for the Advancement of Science)*, *338*(6106), 496–500. https://doi.org/10.1126/science.1227079

[15] Lobbia, R. & Beal, B. (2017) Recommended practice for use of langmuir probes in electric propulsion testing. *Journal of Propulsion and Power*, 33(3):566–581. https://doi.org/10.2514/1.B35531

[16] Herman, D., Shastry, R., Huang, W., Soulas, G., & Kamhawi, H. (2012) Plasma Potential and Langmuir Probe Measurements in the Near-field Plume of the NASA-300M Hall Thruster.

[17] Dannenmayer, K., Kudrna, P., Tichý, M., & Mazouffre, S. (2011) Measurement of plasma parameters in the far-field plume of a Hall effect thruster. *Plasma Sources Science and Technology*, 20(6)https://doi.org/10.1088/0963-0252/20/6/065012

[18] Sheehan, J. & Hershkowitz, N. (2011) Emissive probes. *Plasma Sources Science and Technology*, 20(6)https://doi.org/10.1088/0963-0252/20/6/063001

[19] Sheehan, J., Raitses, Y., Hershkowitz, N., & McDonald, M. (2017) Recommended practice for use of emissive probes in electric propulsion testing. *Journal of Propulsion and Power*, 33(3):614–637. https://doi.org/10.2514/1.B35697

[20] Kemp, R &, Sellen, J. (1966) Plasma potential measurements by electron emissive probes. *Review of Scientific Instruments*, 37(4):455–461. https://doi.org/10.1063/1.1720213

[21] Jameson, K., Goebel, D., Hofer, R., & Watkins, R. Cathode Coupling in Hall Thrusters. *Presented at the 30th International Electric Propulsion Conference, Florence, Italy. 2007*

[22] Sheehan, J., Raitses, Y., Hershkowitz, N., Kaganovich, I., & Fisch N. (2011) A comparison of emissive probe techniques for electric potential measurements in a complex plasma. *Physics of Plasmas*, 18(7)https://doi.org/10.1063/1.3601354

[23] Beal, B &Gallimore, A. (2003). Energy Analysis of a Hall Thruster Cluster.

[24] Shastry, R., Hofer, R., Reid, B., & Gallimore, A. (2009) Method for analyzing E×B probe spectra from Hall thruster plumes. *Review of Scientific Instruments*, 80(6)https://doi.org/10.1063/1.3152218